CrossMark

An image based clump library for DEM simulations

Junxing Zheng[1] · **Roman D. Hryciw**[1] (ID)

Abstract To create realistic virtual soil specimens for Discrete Element Method simulations, a library containing nearly 100,000 "clumps" was developed. A clump essentially models a soil particle. It consists of numerous overlapping spheres in 3D, or circles in 2D, that are tangent to the particle perimeter. By using a unique corner-preserving algorithm based on the classic 2D definition of particle roundness, the clump generation requires many fewer circles than by previous algorithms. In this paper, the clumps are based on 2D images of real soil particles and they are indexed in the library by their roundness R and sphericity S values. A real soil can be simulated by choosing particles from the library to match the soil's actual distributions of R and S. The clumps are also enlarged or reduced to match a desired particle size distribution. The utility of the clump library in parametric studies was demonstrated by direct shear tests on five very different virtual materials created from clumps in the library.

Keywords Discrete element method · Clump library · Particle images · Particle size distribution · Particle roundness · Particle sphericity

List of symbols

A	Particle area
d	Particle size (diameter)

✉ Roman D. Hryciw
 romanh@umich.edu

 Junxing Zheng
 junxing@umich.edu

1 Department of Civil and Environmental Engineering, University of Michigan, 2340 GG Brown, Ann Arbor, MI 48109-2125, USA

d_1	Particle length
d_2	Particle width
D	A fitting parameters in the Rosin–Rammler function
E_c^*	Effective modulus of a clump
E_w^*	Wall modulus in a DEM model
id	Identification number for a clump in the library
n	Porosity of a virtual soil
n_p	Presumed porosity of a virtual soil
n_c	Number of circles in a clump
N	Number of clumps required from the clump library
N_c	Number of the corners around the particle perimeter
T	Shear force
T_p	Shear force at the peak strength
r_i	Radius of the ith corner circle of a particle
r_{ins}	Radius of the maximum inscribed circle in a particle
R	Particle roundness
R_L	Roundness index for a clump in the library
R_m	Mean roundness in an assembly of clumps
S	Particle sphericity
S_L	Sphericity index for a clump in the library
S_m	Mean sphericity in an assembly of clumps
P	Normal force
v	Particle volume
V_t	The test vessel dimension
β_n	Normal critical damping ratio
β_s	Shear critical damping ratio
Δu_x	The horizontal displacement rate at the peak strength state
Δu_y	The vertical displacement rate at the peak strength state

η	A fitting parameters in a two-dimensional Gaussian probability density function
κ^*	Normal to shear stiffness
λ	A fitting parameters in the Rosin–Rammler function
μ	Clump friction coefficient during the shearing stage
ρ	Clump density
Σ	A fitting parameters in a two-dimensional Gaussian probability density function
ϕ_p	Peak angle of internal friction
ψ_p	Peak dilation angle

1 Introduction

All mechanical soil properties fall into two categories: intrinsic and state properties. The intrinsic properties include particle size distribution, particle sphericity, roundness, surface roughness, and properties related to mineralogy such as hardness. State properties include void ratio, effective confining stress and fabric. Intrinsic properties are those that are unaltered by sampling, densification or other disturbance. Abundant studies have shown that soils with similar intrinsic and state properties exhibit similar macro mechanical behavior. Some of the studies include: Eisma [1], Koerner [2], Holubec and d'Appolonia [3], Youd [4], Zelasko et al. [5], Edil et al. [6], Oda et al. [7], Sladan et al. [8], Vepraskas and Cassel [9], Moroto and Ishii [10], Sukumaran and Ashmawy [11,12], Cubrinovski and Ishihara [13], Yasin and Safiullah [14], Santamarina and Cho [15], Cerato and Lutenegger [16], Cho et al. [17], Guo and Su [18], Masad et al. [19], Rouse et al. [20], Bareither et al. [21], Cavarretta et al. [22], Shin and Santamarina [23], Zheng and Hryciw [24] and many others.

The Discrete Element Method (DEM) is commonly used to simulate particulate materials under mechanical loading to investigate micro scale behavior that may not be easily observed or measured in physical tests. Hypothetically, if a virtual soil specimen is created that has the same intrinsic and state properties as a real soil specimen its behavior in a DEM simulation should faithfully mimic the actual physical test. The question then becomes how to reproduce the intrinsic and state properties in the DEM model.

Although major advances have occurred in DEM modeling over the last few decades, the virtual soil specimens often still consist of idealized disks or spheres as they did at the origin of DEMs in the 1970s [25]. Admittedly, disks or spheres have the merits of simple contact detection and force calculation, and therefore low computational cost. However, they oversimplify the geometries of natural soil particles and, as a result, may not accurately simulate the micro or macro behavior of real soils. Therefore, techniques for generating irregular particle shapes to more faithfully reproduce real soil grains have been sought.

Non-spherical particles such as ellipsoids [26–30], spherical cylinders [31], pentagons [32], rounded-cap elongated rectangles [33], polyhedrons [36–41], and Non-Uniform Rational Basis-Splines (NURBS) [41] have been developed and utilized in DEM. 'While these have been improvements over perfect disks or spheres, they are still idealized geometries. An improvement towards simulating more realistic particle geometries uses clumps of overlapping spheres (or circles) to create various irregular shapes. Many clump generation algorithms have been proposed including the methods of Ferellec and McDowell [41] and Taghavi [42]. The basic procedures of these algorithms are similar; they exhaustively fit many interior circles (or spheres) to the particle boundary then eliminate some of the less needed circles (or spheres) to reduce computational effort. However, the criteria used to eliminate the circles vary from particle to particle depending on particle size, angularity and image magnification [43]. Therefore, users must subjectively tune the criteria parameters for each clump to achieve an optimal number of circles to represent each particle. Consequently, considerable effort is needed to generate a statistically significant large number of clumps to reproduce a natural soil specimen in a DEM model.

Recently, Zheng and Hryciw [43] developed a two dimensional (2D) "corner-preserving" clump generation algorithm. They did so by utilizing and extending the classic definition of particle roundness developed by Wadell [44–46]. The corner preserving algorithm significantly reduces the need for user intervention in the clump generation process and therefore minimizes subjectivity and enhances the accuracy of the generated clumps. Compared to previous approaches, the corner-preserving algorithm uses many fewer circles to represent a soil particle thereby also improving computational efficiency.

To reproduce an actual soil specimen perfectly, the corner-preserving algorithm could conceivably be used to generate as many clumps as there are particles in the soil specimen. To do so would require an image of every soil particle. It is certainly worth considering if such a large number of particle images must necessarily be collected each time a new soil is to be simulated. Instead, could virtual soil specimens be constructed from a permanent library of clumps based only on desired distributions of particle shapes and sizes? The desired distributions could be to model an actual soil specimen for which the size distribution would be determined either by conventional sieving or image analysis and for which the shape distribution would be determined by image analysis on a statistically representative number of particles. Alternatively, the library could be used for parametric studies without an actual soil to be modeled.

Some intrinsic properties including surface roughness and hardness are accounted for through defined mechanical

model parameters such as the contact friction coefficient and particle stiffness. The remaining parameters including the distributions of particle size, particle sphericity and roundness have limitless possibilities and must be preserved by the clump geometries. The question narrows down to how to create appropriate clump geometries to satisfy the desired distributions. As mentioned earlier, exhaustively reproducing all of a specific sand specimen's particles by clumps is not an efficient approach. Creation of the clump library would eliminate the need for reproducing tens of thousands of particles for each simulation.

This paper describes the development of a large permanent clump library for use with DEMs. It shows how the library was constructed from numerous previously collected images of individual sand particles and how it may be used. At the present time, the library consists of only 2D particles developed from images of 2D particle projections. While soils must naturally be simulated by 3D clumps in DEMs, there are compelling reasons and distinct advantages to first developing a 2D particle library. First, the classic definitions of R and S are based on 2D particle projections and there is a long history of their usage. The corner-preserving algorithm is also presently only developed for 2D. It is easier to demonstrate the construction and usage of a 2D library. Results of 2D simulations are easier to visualize and interpret. Finally, the computational power required to create and test the library is far less demanding. Indeed, a 3D DEM simulation using a statistically valid number of clumps to faithfully simulate a real soil problem is still somewhat unrealistic.

2 Intrinsic soil properties

Based on 2D particle projections, particle size will be defined in this paper as the diameter, d, of circle having the same area, A, as the soil particle:

$$d = 2 \times \sqrt{\frac{A}{\pi}} \qquad (1)$$

Particle shape could be characterized at three observation scales according to Barrett [47]. From largest to smallest scale, the descriptors are sphericity (S), roundness (R), and surface roughness. Sphericity describes how close the overall particle shape is to a perfect circle (or sphere). For 2D projections, the S has been defined differently by Tickell [48], Wadell [46], Santamarina and Cho [15], Altuhafi et al. [49], and Krumbein and Sloss [50]. Zheng and Hryciw [51,52] compared the various definitions and found the one proposed by Krumbein and Sloss [50] to be the most practical for describing S. Cho et al. [17] and Zheng and Hryciw [53] showed that various mechanical properties of soils including packing, compressibility, critical state friction angle, and
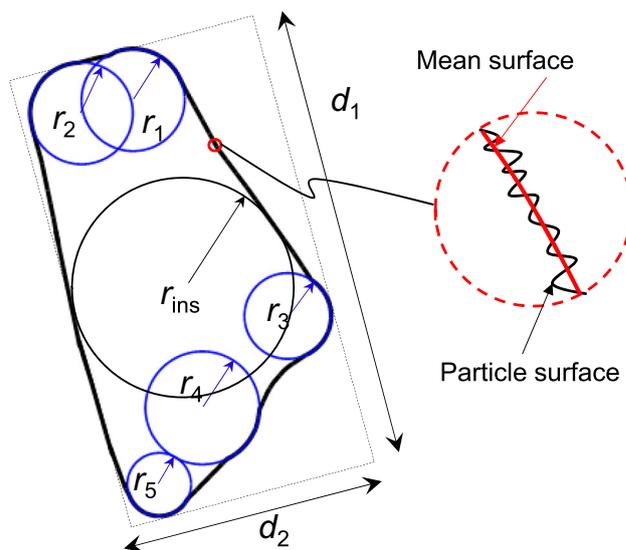

Fig. 1 Geometric parameters for defining various intrinsic properties

small strain modulus are closely related to the S of Krumbein and Sloss [50]. Therefore, their simple definition of sphericity is adopted for this study:

$$S = \frac{d_2}{d_1} \qquad (2)$$

where d_1 and d_2 are the length and width of a particle respectively as shown in Fig. 1.

At the second observation scale, R describes the sharpness of corners on soil particles. The definition of particle roundness was first proposed by Wadell [18–20] as the ratio of the average radius of curvature of the corners of a particle to the radius of the maximum inscribed circle as shown in Fig. 1:

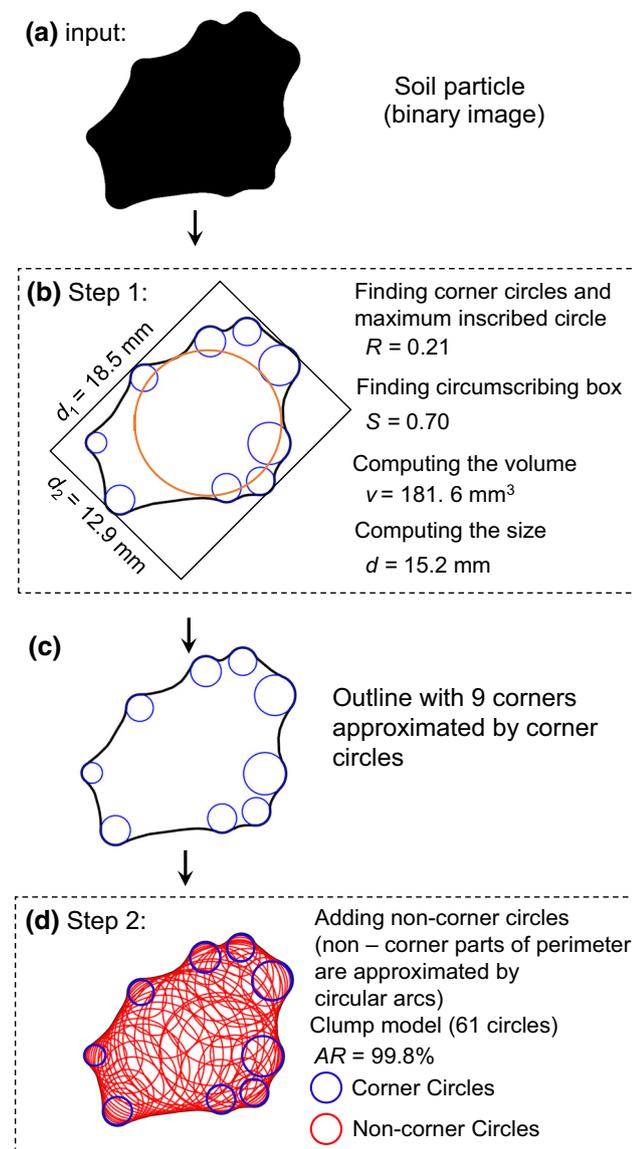$$R = \frac{\sum_{i=1}^{N_c} r_i \Big/ N_c}{r_{ins}} \qquad (3)$$

where r_i is the radius of the ith corner circle; r_{ins} is the radius of the maximum inscribed circle; and N_c is the number of the corners around particle perimeter. Determination of Wadell roundness was recently automated using a computational geometry algorithm developed by Zheng and Hryciw [51]. The algorithm was verified by Zheng and Hryciw [51,52] using all of the particles in the R reference charts provided by Krumbein [54], Krumbein and Sloss [50] and Power [55].

Surface roughness describes the soil surface at smallest observation scale as shown in Fig. 1. In DEM simulations, while d, S and R can be preserved exactly by the geometries of the generated clumps, surface roughness must be represented by the contact frictional coefficient μ. The determination of μ will be addressed later in this paper.

3 Corner-preserving algorithm for creating clumps

The corner preserving algorithm for creating 2D clumps begins with a binary particle projection such as shown in Fig. 2a. Two steps are involved in creating a clump to represent the particle silhouette. In step 1, the computational geometry algorithm developed by Zheng and Hryciw [51] identifies corners on the particle perimeter and fits circles to them as shown in Fig. 2b. The maximum inscribed circle and minimum circumscribing box are also determined. At this point, d, A, R and S can be computed. In two-dimensional DEM models, the third dimension is of unit width and therefore the particle volume is $V = A \times 1$.

The particle perimeter along with its corner circles (Fig. 2c) are the input to the second stepwhere the non-corner

(a) input:

Soil particle
(binary image)

(b) Step 1:

$d_1 = 18.5$ mm

$d_2 = 12.9$ mm

Finding corner circles and maximum inscribed circle
$R = 0.21$

Finding circumscribing box
$S = 0.70$

Computing the volume
$v = 181.6$ mm³

Computing the size
$d = 15.2$ mm

(c)

Outline with 9 corners approximated by corner circles

(d) Step 2:

Adding non-corner circles (non – corner parts of perimeter are approximated by circular arcs)
Clump model (61 circles)
$AR = 99.8\%$

◯ Corner Circles

◯ Non-corner Circles

Fig. 2 The corner-preserving algorithm

portions of the particle perimeter are identified and fitted with additional circles as shown in Fig. 2d. In the end, the soil particle perimeter is represented by a cluster of several corner circles and many non-corner circles. The example particle shown in Fig. 2d was approximated by a total of 61 circles of which 9 are corners circles and 52 are non-corner circles.

In the process of clump generation, various actual intrinsic soil properties including d, R and S are computed for each particle, i.e. clump. These parameters will serve as unique indices for the clumps in the library.

4 Clump library construction

To date, a total of 98,489 images of real soil particles have been collected and modeled by clumps using the 2D corner-preserving algorithm. The "clump library" includes a wide range of particle sizes, angularities, and sphericities. The library can be expanded by adding more clumps. Ten select clumps from the library are shown in Fig. 3. The listed R and S values have been rounded and saved in the library with two decimals. The number of circles used to construct each clump (n_c) is also shown. Having complex surface structures, the angular particles clearly require more circles to approximate them. Very elongated (low S) particles also naturally need more circles. Each clump is archived in the library by an index "$R_L\_S_L\_id$" consisting of three integers as shown in Fig. 3. The R_L and S_L are hundred-folds of the computed R and S values respectively. Since many clumps may have the same R_L and S_L values, the third parameter "id" is used to discriminate them. The combination of these three digits is able to catalog an unlimited number of clumps in the library. The information stored in the library for each clump also includes *basic* and *structural* information. The basic information includes the clump volume v and size d. The structural information includes the total number of circles n_c, as well as the radius and center location of each circle.

A convenient map of the clump library is shown in Fig. 4. The locations of clumps in the library are determined by their R_L and S_L values. As just mentioned, many particles may possess the same R and S combination. Thus, multiple clumps may exist at one map location. For example, there are 34 clumps at the spot $(R_L, S_L) = (55, 63)$ in Fig. 4. The 34 clump are distinguished by the id numbers from 55_63_1, 55_63_2, … up to 50_63_34.

In Fig. 4, the library has 100×100 locations but not all locations contain clumps. Locations at $S_L < 20$ and $R_L < 15$ barely have any occupants. This is somewhat expected. Extremely elongated and angular particles are rare in nature since such particles are vulnerable to breakage [56]. Histograms of the clumps for R_L and S_L are shown in Fig. 5a, b respectively. Angular particles have more complex outlines than rounded particles and the variability of parti-

R	S	n_c	R	S	n_c	R	S	n_c	R	S	n_c	R	S	n_c
0.11	0.86	83	0.27	0.76	64	0.48	0.78	41	0.70	0.76	17	0.86	0.95	16
Index: 11_86_1			27_76_1			48_78_1			70_76_1			86_95_1		

R	S	n_c	R	S	n_c	R	S	n_c	R	S	n_c	R	S	n_c
0.47	0.20	48	0.50	0.28	56	0.11	0.43	86	0.46	0.47	30	0.65	0.66	21
Index: 47_20_1			50_28_1			11_43_1			46_47_1			65_66_1		

Fig. 3 Ten selected clumps from the library
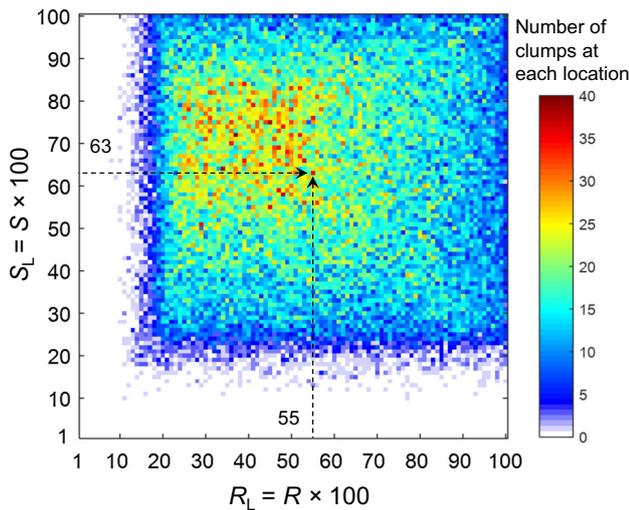
Fig. 4 Map of the clump library

cle shapes increases with increasing angularity (decreasing roundness). Therefore, more angular particles in the range $20 < R_L < 50$ were deliberately collected for the library as shown in Fig. 5a. The S_L histogram in Fig. 5b reflects the prevalence of shapes in the range $60 < S_L < 80$ found in nature.

5 Steps in virtual soil specimen creation

The DEM virtual soil specimen creation process includes four steps as shown in Fig. 6.

Step 1: Given a specific soil, users must characterize it to obtain particle d, S, and R distributions. The d can be determined by traditional sieve analysis or by spectral of optical techniques such as the University of Illinois Aggregate Imaging System (UIAIA) [57–60], the Aggregate Imaging System (AIMS) [61–64], the Translucent Segregation Table system (TST) [65,66], the QICPIC system [49], the Vision cone penetrometer (VisCPT) [67–70] and Sedimaging [71]. The particle shape distributions including R and S distributions can be computed using computational geometry methods from either two-dimensional binary projections [51] or from images of three-dimensional particle assemblies [52]. This study found that 200 particles were sufficient to provide satisfactory characterization of a real soil. However, users can create their own particle size and shape distributions to construct a customized virtual soil specimen.

Step 2: Users must input the testing vessel dimensions, a traditional weight-based particle size distribution (real or assumed) and a target packing porosity n_p. For normal (not gap-graded) soils, weight (or volume) based particle size distributions may be fitted with the Rosin–Rammler function [72]:

$$V(d) = 1 - \exp\left[-\left(\frac{d}{D}\right)^{\lambda}\right] \qquad (4)$$

in which D and λ are the fitting parameters related to the 50% particle size by weight, D_{50} and the coefficient of uniformity, C_u respectively. The total
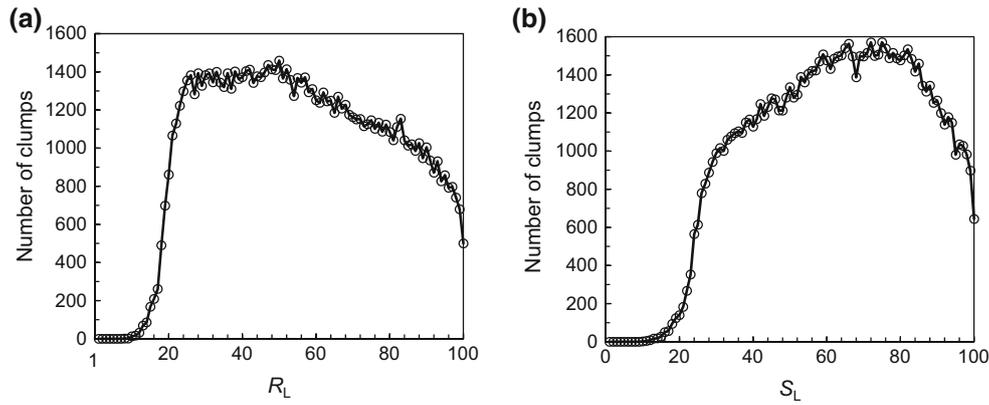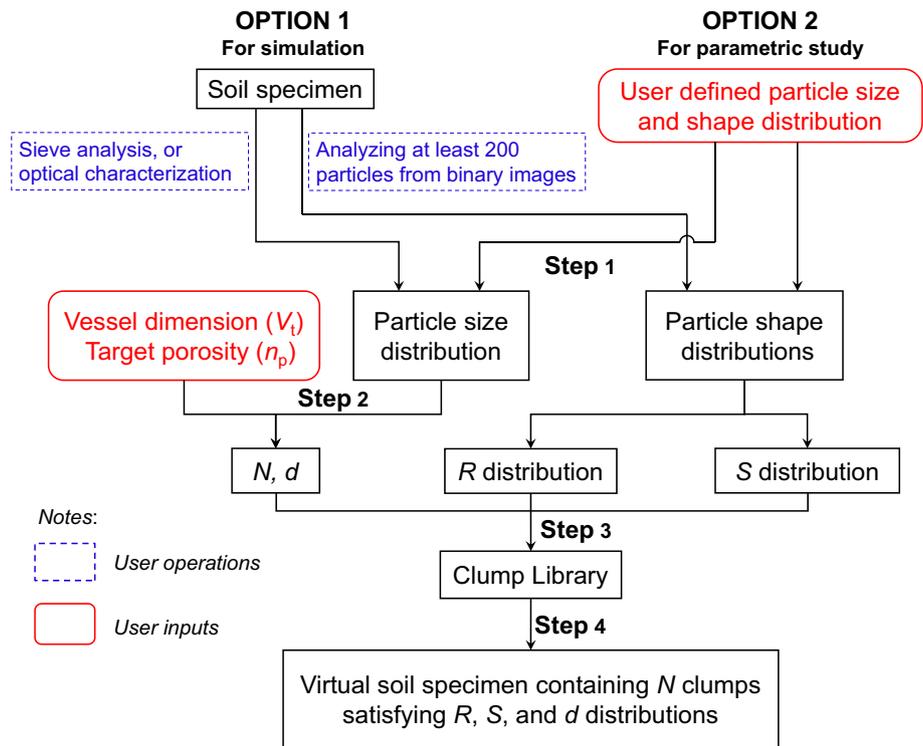
Fig. 5 The number of clumps in the library versus R_L and S_L

Fig. 6 Overview of the virtual specimen preparation technique

number of particles (N) required to fill the virtual testing vessel at porosity n_p and their distribution by size (d) are then computed.

Step 3: The distributions of R and S are unwieldy in discrete form. As such, they may be modeled by a two-dimensional Gaussian probability density functions (PDF):

$$f(x|\mu, \Sigma) = \frac{1}{2\pi} \frac{1}{|\Sigma|^{1/2}}$$
$$\times \exp\left\{-\frac{1}{2}(x - \eta)' \Sigma^{-1}(x - \eta)\right\} \tag{5}$$

where x is a matrix of R and S values of k evaluated particles:

$$x = \begin{bmatrix} R_1, R_2, R_3, \ldots, R_k \\ S_1, S_2, S_3, \ldots, S_k \end{bmatrix};$$

η is the mean vector of R and S values:

$$\eta = \begin{bmatrix} \eta_R \\ \eta_S \end{bmatrix},$$

and Σ is the covariance matrix: $\Sigma = \begin{bmatrix} \Sigma_{RR} & \Sigma_{RS} \\ \Sigma_{SR} & \Sigma_{SS} \end{bmatrix}$.
The program retrieves the N clumps from the library based on a soil specimen's R & S PDF.

Step 4: The N clumps are input to the DEM code to assemble the virtual soil specimen. Several DEM codes are compatible with clump simulation including the commercial code Particle Flow Code (PFC) by Itasca [73] and open source codes including the Large-scale Atomic/Molecular Massively Parallel Simulator (LAMMPS) [74] and its improved version General Granular and Granular Heat Transfer Simulations (LIGGGHTS) [75]. The PFC by Itasca was used in this study.

6 Example of virtual soil specimen creation

The process used to prepare virtual specimens for DEM simulation of direct shear testing is demonstrated using an Indiana Beach sand at dense and loose conditions.

In Step 1 traditional sieve analysis was used to determine the particle size distribution of an Indiana Beach sand. The result is shown in Fig. 7a as a traditional weight-based cumulative distribution. A total of 200 particles were then randomly selected from the physical specimen. The particles were spread on a flat surface and binary images were captured. Zheng and Hryciw's [51] computational geometry method was used to compute R and S values for every particle. The cumulative distributions of R and S values by number of particles are shown in Fig. 7b, c.

In Step 2, the particle size distribution shown in Fig. 7a is fitted using Eq. (4). The values $D = 1.2$ and $\lambda = 2.3$ were found to match the Indiana Beach Sand sieving results very well. The curve is discretized into 200 equal fractions as shown in Fig. 8. Each fraction represents a volume increment of $\Delta V = 0.5\%$. The particle size d_i representing the ith volume fraction can be back-calculated using Eq. (4). Knowing d_i, the volume v_i of each particle in the ith volume fraction can be computed as shown in Fig. 8.

To determine the number of particles in the ith fraction, the volume of solids in this fraction must be computed as $V_t(1 - n_p)\Delta V$ where V_t is the testing vessel volume and n_p is the porosity, both specified by the user. Finally, the number of particles required for the ith volume fraction can be expressed as:

$$num_i = \frac{V_t \times (1 - n_p) \times \Delta V}{v_i} \tag{6}$$

For example, the volume of a 2D shear box V_t used in this study was $100 \times 48 \times 1 = 4800$ mm^3 and the target porosity n_p was set to 0.2. The particle size of ith volume fraction
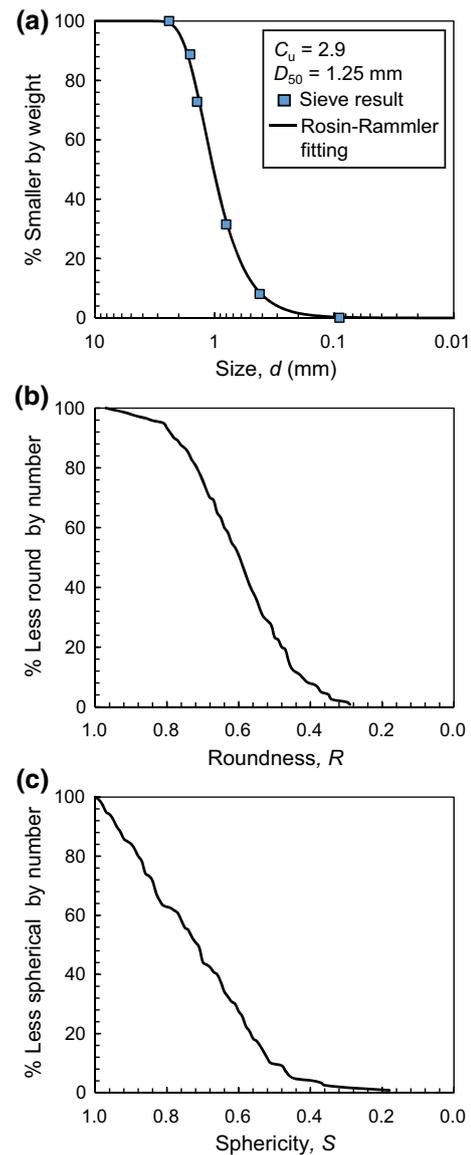
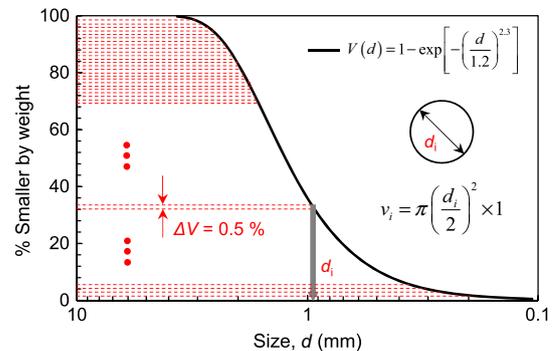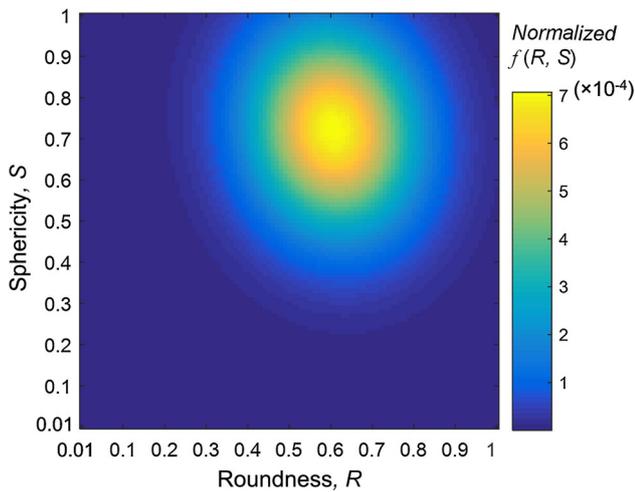**Fig. 7** Characterization of Indiana Beach sand

Fig. 8 Discretization of particle size distribution curve

was 0.94 mm. Based on Eq. (6), $num_i = 27$ particles were required to model this fraction. This computation is repeated

Fig. 9 The normalized probability density map

Fig. 10 Number of clumps retrieved from each location in the library for the example

for each volume fraction. The total number of required particles N to fill the direct shear box will be the sum of num_i. In this case, N was 12,518.
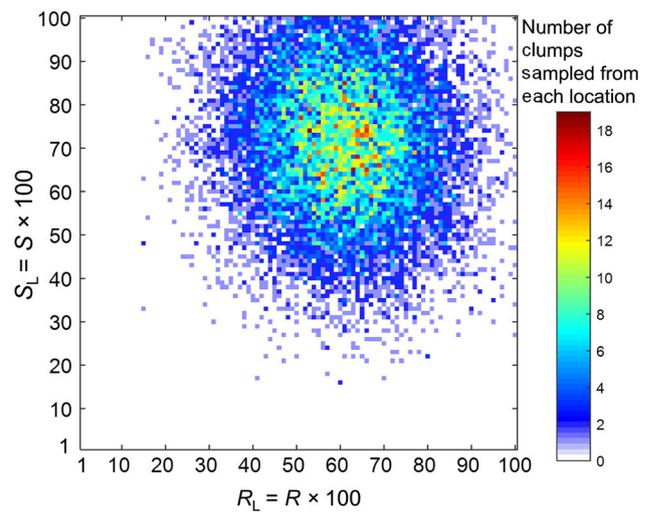
In Step 3, N clumps are retrieved from the library according to their R and S distributions as follows. The R and S distributions in Fig. 7b, c are fitted to the two-dimensional Gaussian probability density function, Eq. (5). In this example, η and Σ were computed as:

$$\eta = \begin{bmatrix} 0.61 \\ 0.72 \end{bmatrix} \text{ and } \Sigma = \begin{bmatrix} 0.0193 & -0.0019 \\ -0.0019 & 0.0293 \end{bmatrix}.$$

These were inserted into Eq. (5) to determine the probability density function f which is plotted in Fig. 9. This $f(R, S)$ map in Fig. 9 dictates the sampling probability for each location in the clump library shown in Fig. 4. The program will sample the library N times as was determined in Step 2. It should be noted that one location can be sampled multiple times. The number of stored clumps at each location in Fig. 4 will generally not be the same as the needed number from that location. Statistically speaking, if the total number of particles needed from a single location in the library is m and the number of clumps at that location is k, then each clump from that library location will be used, on average, m/k times.

Using the above procedure, $N = 12,518$ clumps were retrieved from the library for the Indiana Beach sand. Figure 10 shows the number of clumps sampled from each location in the library.

The d values obtained in Step 1 and 2 are now randomly assigned to the N generated clumps. This is done by enlarging or reducing each clump to meet its assigned d value. For example, the 15.2 mm clump shown in Fig. 2 is one of the clumps retrieved from the library. The particle was assigned a size of $d = 0.94$ mm. Therefore, the clump in

Fig. 2 is reduced by a factor of 0.94/15.2 to achieve the target d. The final size and shape information for this clump is $(R_i, S_i, d_i) = (0.21, 0.70, 0.94 \text{ mm})$.

The d, R and S distributions of clumps in the DEM model are compared to the distributions of the original soil in Fig. 11. The DEM model successfully reproduced the target distributions of the original soil.

In Step 4, the N generated clumps were input into PFC and rained into a direct shear box. The top cap was added and the specimen was consolidated under a normal stress of 100 kPa. A linear contact model was used in this simulation. The model parameters were set as follows: the clump density ρ was 2650 kg/m^3; the effective modulus of the clumps E_c^* was 5×10^8 N/m^2; the effective modulus of the wall E_w^* was 5×10^9 N/m^2; the normal-to-shear stiffness ratio κ^* was 1.5; both normal and shear critical damping ratio (β_n and β_s) of the clumps were 0.5. To achieve a dense packing state, the friction coefficients for both the clump–clump and clump–wall interfaces were set to zero. The specimen is shown after consolidation in Fig. 12a. Two small square areas are enlarged and shown in Fig. 12b, c. As observed, each clump possesses a unique size and shape.

After consolidation, the final porosity n was 0.13. It should be noted that the n value after consolidation is not necessarily equal to the initially specified n_p. The n_p is a presumed value for initially computing the number of clumps required to be retrieved from the library. The n after consolidation may be different than n_p. Correspondingly, the final vessel height may also be different from the previously specified value to accommodate the change in porosity due to consolidation. In this example, the height of the specimen was 44 mm after consolidation instead of previously specified 48 mm dimension. It was found in this study that such small changes in
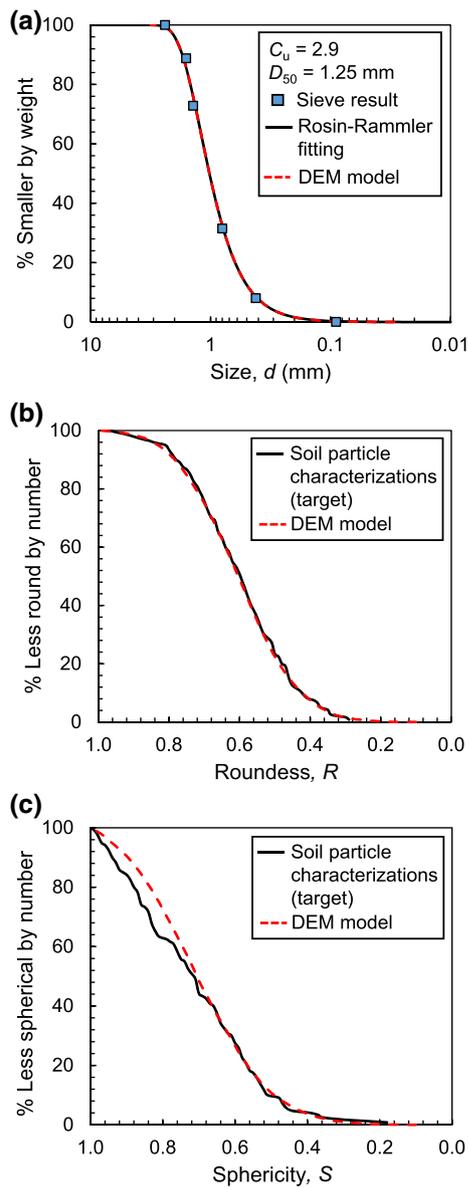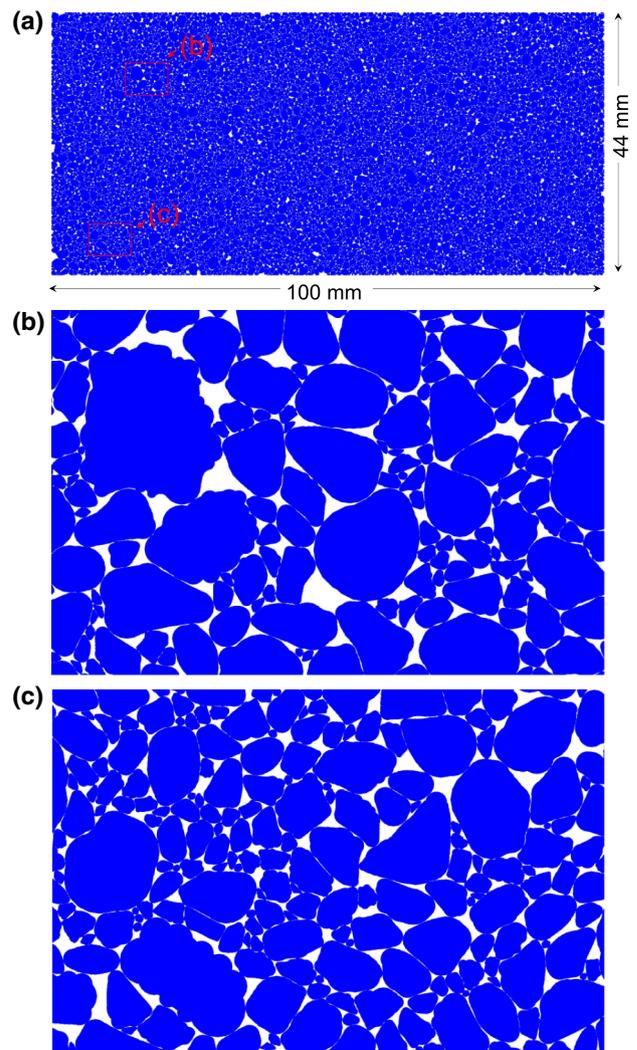
Fig. 11 Sand size and shape distributions generated from the clump library compared to their target distributions

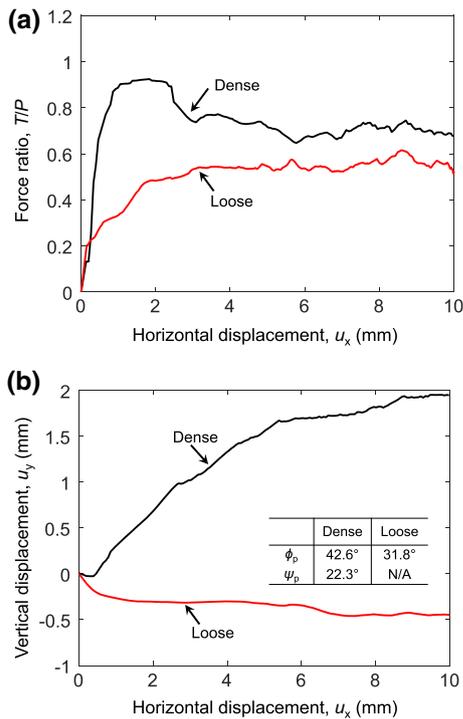
Fig. 12 The generated DEM model at a dense condition

7 DEM simulation of direct shear tests

The normal stress was kept as 100 kPa during specimen shearing. The clump–clump and clump–wall contact friction coefficients were set to 0.50 and 0.95 respectively. The upper half of the box was fixed and the lower half was displaced at a constant velocity of 0.004 mm/s. The top wall was continuously adjusted via a serve-control mechanism [73] to maintain the constant vertical normal stress during shearing. The horizontal displacement, vertical displacement, and shear force results are shown in Fig. 13.

The peak friction angle and dilation angle can be computed from the test curves as

$$\phi_p = a \tan\left(\frac{T_p}{P}\right) \tag{7}$$

$$\psi_p = a \tan\left(\frac{\Delta u_y}{\Delta u_x}\right) \tag{8}$$

shear box height did not affect the final simulation results. Naturally, the n_p should be as close to n as possible. Therefore, steps 1–4 could be repeated using the resulting n value as the new n_p. Readers are encouraged to do so if they feel it is necessary. However, in this study, n_p was fixed at 0.2 and was not adjusted.

To achieve a loose packing condition, the friction coefficient for both the clump–clump and clump–wall interfaces were set to 0.3 for the consolidation stage. The final porosity n was 0.2 which is the same as the presumed value n_p. All other steps in setting up the loose condition were the same as for the dense state.

(a)

(b)

Fig. 13 DEM simulations of Indiana Beach sand at dense and loose conditions

where P is the normal force and T_p is the shear force at the peak; Δu_x and Δu_y are the horizontal and vertical displacement rates at the peak strength state. The resulting ϕ_p and ψ_p are listed in Fig. 13.

8 Clump library usage in parametric studies

Direct shear tests on five additional 2D versions of soils including 30A, Crushed Gabbro (CG), Leighton Buzzard (LB), Class IIA (IIA), and Glass Beads (GB) were also simulated to demonstrate the versatility of the clump library. The 30A and Crushed Gabbro are very angular and crushed angular soils respectively. The Leighton Buzzard is a subangular soil frequently used in research as reported by Lings and Dietz [76] and Jewell [77]. The Class IIA and Glass Beads are subrounded and rounded materials respectively. The particle size distribution of Leighton Buzzard (LB) shown in Fig. 14b was extracted from Lings and Dietz [76]. The particle size distributions of the remaining four sands shown in Fig. 14a, b were determined through sieving analysis. The dashed lines are the Rosin–Rammler curves fitted to the sieving data. The fitting parameters D and λ are summarized in Table 1. The volume of the shear box V_t was set to $100 \times 48 \times 1 = 4800$ mm^3 and the target porosity n_p was set to 0.2 for all of the test simulations. The resulting numbers

of particles (N) required to fill the direct shear box for the five soils are reported in Table 1.

For each soil except the Glass Beads, 200 particles were characterized to determine their R and S distributions. The results are shown as solid lines in Fig. 14c, d. The mean R and S values (R_m and S_m) are listed in Table 1. These solid lines were used to fit two-dimensional Gaussian distributions of R and S using Eq. (5) for retrieval of clumps from the library. The resulting R and S distributions of the picked clumps are plotted as dashed lines in Fig. 14c, d. They agree well with the target distributions. For the Glass Beads, both R and S are equal to 1.0 therefore perfect disks were used in the simulation. The model parameters including ρ, E_c^*, E_w^*, κ^*, β_n, and β_s were the same as used in the earlier simulation of Indiana Beach sand. Only dense conditions were simulated. Therefore, the friction coefficient μ was set to zero for the consolidation stage and to 0.5 for the shearing stage. The normal stresses were set to 100 kPa. The porosities n of the five sands after consolidation are listed in Table 1.

The simulation results are shown in Fig. 15 while the ϕ_p and ψ_p values are plotted in Fig. 16. As shown both ϕ_p and ψ_p increase with decreasing R (increasing angularity) which agrees with the experimental observations of Santamarina and Cho [35], Cho et al. [37], Bareither et al. [56] and countless others.

Although average S values of natural soils fall in a narrow range of 0.6–0.8 [56], it would be interesting to observe the behavior of soils having low S. This is easily facilitated using the clump library. Two virtual soils were created using the Class IIA soil but defining two additional new S distributions as shown in Fig. 17: $S_m = 0.52$ and $S_m = 0.32$. The size and R distributions as well as other parameters were maintained the same as in the original Class IIA. After consolidation, the porosity values were expectedly different: the elongated soils had larger n. The simulation results from these newly created virtual soils are shown in Fig. 18. The computed ϕ_p and ψ_p for each test are shown in Fig. 19. Both ϕ_p and ψ_p increase as S decreases suggesting elongated particles increase strength and dilation. The same laboratory observation was also made by Santamarina and Cho [35] and Cho et al. [37].

To investigate the importance of particle gradation, the parameters D and λ for the Leighton Buzzard sand were changed to create a virtual Well-Graded Leighton Buzzard sand (WGLB) having a C_u of 8.7. The particle size distribution curve for WGLB was added to Fig. 14b. The fine portion smaller than D_{10} (0.15 mm) was ignored because it would dramatically increase the total number of clumps, thereby exceeding current computational ability. The R and S distributions and the remaining parameters were maintained the same as they were for the original Leighton Buzzard sand as listed in Table 1. The DEM simulation results show that strength was enhanced slightly by increasing C_u from 1.3 (LB) to 8.7 (WGLB) as shown in Fig. 20. Kokusho et al.

Fig. 14 Intrinsic property distributions of the simulated soils
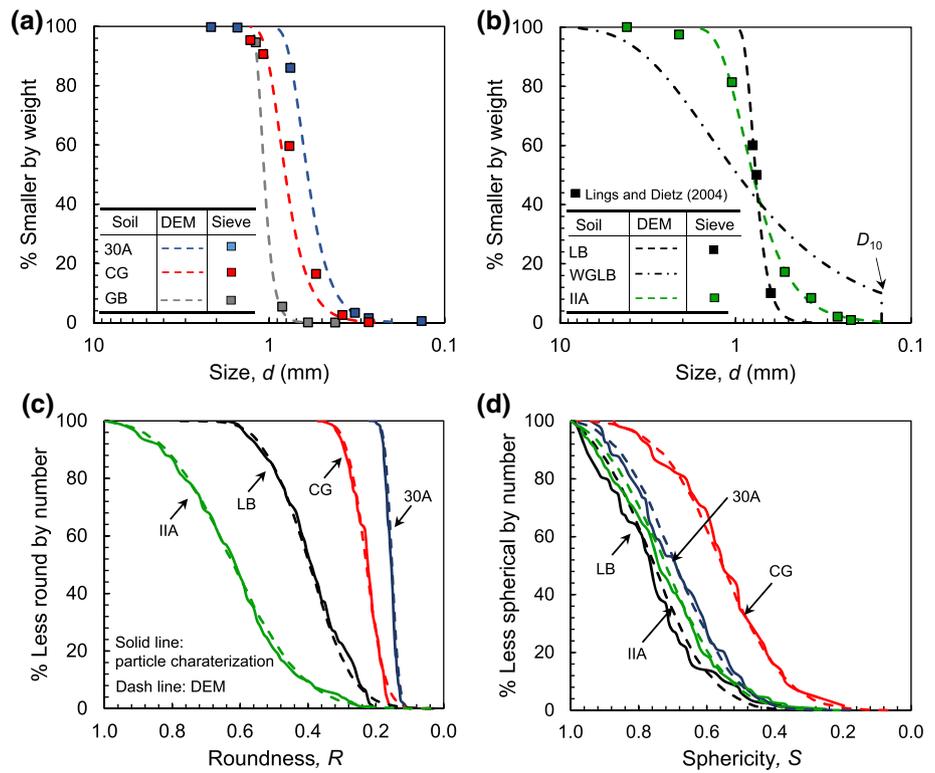
Table 1 The parameters of virtual soils in DEM simulations

Soil	Gradation					Shape		DEM
	D_{50} (mm)	C_u	D	λ	N	R_m	S_m	n
30A	0.58	1.5	0.67	5	15,681	0.15	0.69	0.21
CG	0.80	1.5	0.87	5	9196	0.23	0.56	0.19
LB	0.78	1.3	0.80	9	8802	0.41	0.76	0.15
IIA	0.80	1.9	0.90	3	13,549	0.62	0.72	0.13
GB	1.00	1.1	1.10	10	4570	1.00	1.00	0.14
IIA_0.52[†]	0.80	1.9	0.90	3	13,549	0.62	0.52	0.15
IIA_0.32[†]	0.80	1.9	0.90	3	13,549	0.62	0.32	0.19
WGLB[†]	0.97	8.7	1.40	1	38,696	0.41	0.76	0.11

D_{50} is the 50% size by weight; σ_n is normal stress; μ is clump–clump friction coefficient during the shearing stage; n is porosity after consolidation, N is number of generated clumps; R_m and S_m are the mean values; [†] means those virtual soils are created by author-defined intrinsic properties

[78] performed a series of laboratory tests on sands with different C_u values and found that shear strength could either increase or decrease with increasing C_u depending on particle crushability. If particles are not crushable, the shear strength will increase with increasing C_u while the opposite trend was observed for crushable particles. The crushing of particle will suppress the relative movement and overriding of particles resulting in smaller strength and dilatancy. In this study, both ϕ_p and ψ_p increase with C_u because the clumps were not allowed to crush. This agrees with Kokusho et al.'s [78] observation.

9 Discussion

1. The current 2D clump library consists of 98,489 geometries. In the real world, every particle, particularly if it is angular, has a unique geometry. Furthermore, even for the same particle, different scanning direction will yield different projected 2D geometries. Therefore, the 2D library obviously cannot include all possible particle geometries. However, as discussed earlier, many studies have shown that different soils with similar intrinsic properties will exhibit similar macro-mechanical behavior
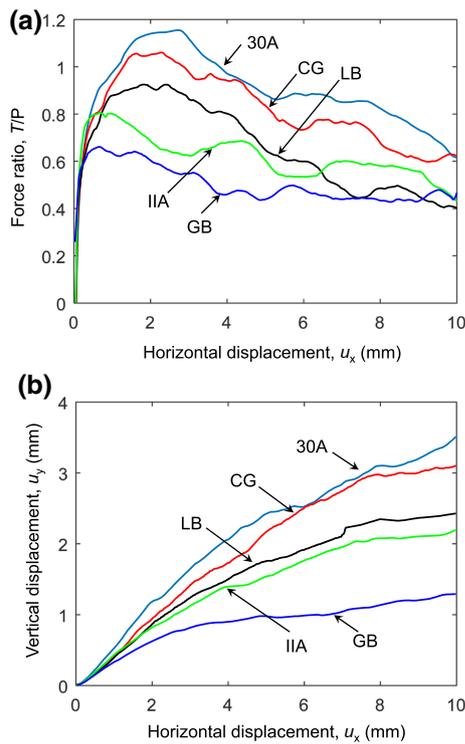
(a)

(b)

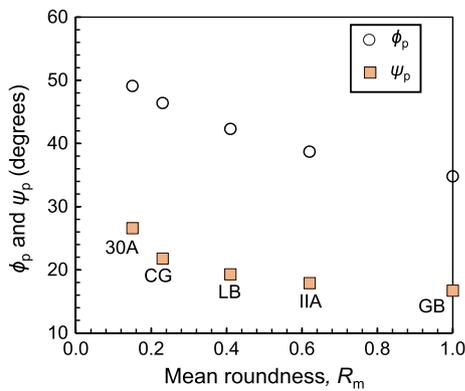**Fig. 15** DEM simulations of five sands with different roundnesses

Fig. 16 The effects of roundness by DEM simulations

Fig. 17 Sphericity distributions of actual and three virtual Class IIA specimens

(a)

(b)
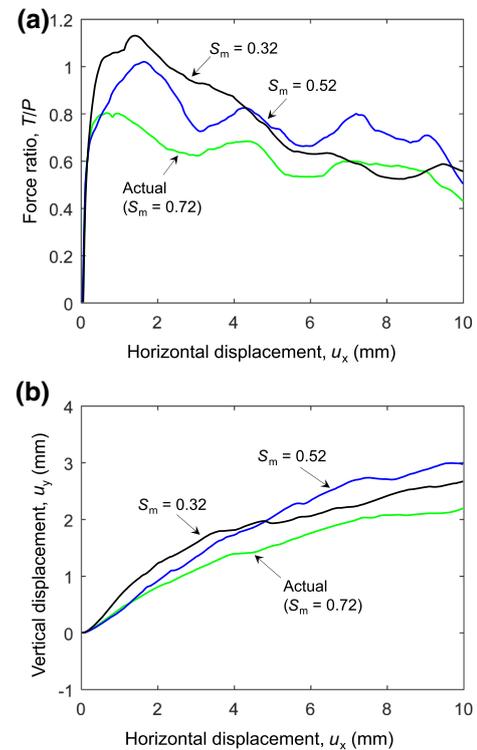
Fig. 18 Simulations of Class IIA at three sphericities

under the same state conditions. The 2D library does not aim to exhaustively contain all possible particle geometries encountered in nature. Rather, it contains sufficient geometries for reproducing all possible intrinsic parameter distributions.

2. To simplify image acquisition, the clumps in the library were generated from images of particles spread out on a flat surface. As such, the particles are more likely to have been displaying their maximum area projections. While it would appear that such images are most reflective of particles lying in a depositional plane, the library does not ascribe any specific orientation to the clumps. As such,
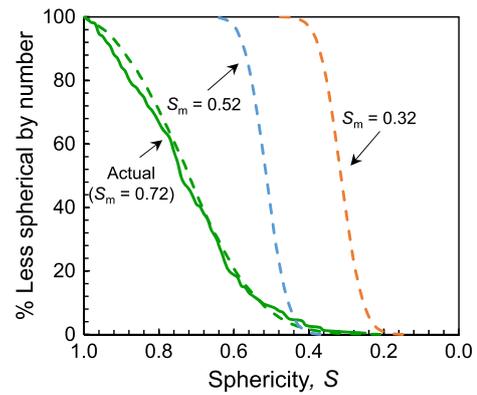
the clumps in the library may be used for simulating other orientations having appropriate user-specified R and S distributions.

3. The shortcomings of two-dimensional DEMs are well known: 2D particles have only three degrees for freedom compared to six in real soils. Nevertheless, as discussed in the Introduction, 2D DEMs hold several attractive benefits including computational efficiency, simplicity of model preparation and easier visualization of particle motions. Furthermore, the direct linkage between Wadell's classic 2D definition of particle roundness, through the corner-preserving algorithm, preserves the
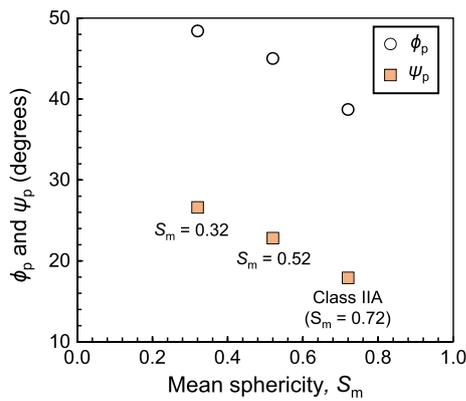
Fig. 19 The effects of sphericity by DEM simulations
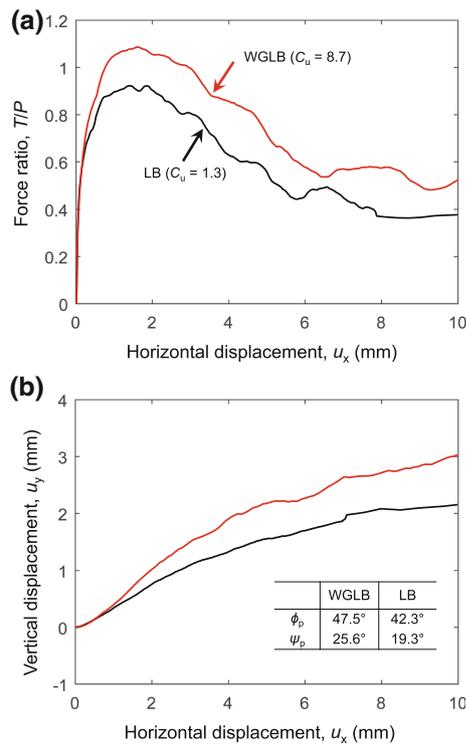
Fig. 20 The effects of gradation in DEM simulations

exact shape of particles and facilitates more efficient clump generation. In the future, Wadell's definition of roundness could and should be extended to 3D thus providing a basis for 3D clump generation. Such clumps would require hundreds of spheres making them still computationally unrealistic at the present time. Nevertheless, even in 2D, the value of clump libraries towards parametric study of particle micromechanics is significant.

10 Conclusions

A library consisting of almost 100,000 two-dimensional clumps was developed for use with Discrete Element Methods. Each clump was created from a binary image of a sand particle. The particles in the clump library are indexed by their values of roundness (R) and sphericity (S). The R follows the classical definition of roundness developed by Wadell [44–46] while S follows a simple definition proposed by Krumbein and Sloss [50]. A previously developed computational geometry technique fits circles to a particle's corners thereby facilitating the computation of R. A previously developed "corner-preserving" algorithm fits many additional interior circles to the particle perimeter. The particles in the clump library are based on sands taken from many sources and thus they possess a wide range of R and S values.

The clump library may be used to simulate an actual soil whose particle size distribution is determined by either sieving or by image analysis and whose distributions of R and S are determined by computational geometry on 200 randomly selected particles. The particle size distribution is fitted to the Rosin–Rammler function while the R and S distributions are smoothed by a two-dimensional Gaussian probability density function. The clump library may also be used in parametric studies in which the particle size, R and S distributions are designed by the user. In either case, the clumps are picked from the library to create a virtual soil specimen according to their Gaussian distributions of R and S. The clump sizes are then adjusted to match the desired particle size distribution. Example problems showed very good matches between the actual distributions of particle size, R and S and the distributions of these intrinsic properties in a virtual specimen composed of clumps from the library.

DEM simulations of direct shear tests on five vastly different sands were performed using the clump library. The simulation results qualitatively match well known trends documented in the literature. Both ϕ_p and ψ_p were observed to increase with decreasing R (increasing angularity), decreasing S, and increasing C_u (for non-crushable soils). Those simulations illustrate the usefulness and versatility of the clump library in creating virtual specimens possessing various shapes and particle gradations.

Compliance with ethical standards

Conflict of interest The authors declare that they have no conflict of interest

References

1. Eisma, D.: Eolian sorting and roundness of beach and dune sands. Neth. J. Sea Res. **2**(4), 541–555 (1965)
2. Koerner, R.M.: Limiting density behavior of quartz powders. Powder Technol. **3**(1), 208–212 (1970)
3. Holubec, I., D'Appolonia, E.: Effect of particle shape on the engineering properties of granular soils. In: Evaluation of Relative Density and its Role in Geotechnical Projects Involving Cohesionless Soils. pp. 304–315. ASTM International, New York (1973)
4. Youd, T.L.: Factors controlling maximum and minimum densities of sands. ASTM Spec. Tech. Publ. **523**, 98–112 (1973)
5. Zelasko, J.S., Krizek, R.J., Edil, T.B.: Shear behavior of sands as a function of grain characteristics. In: Istanbul Conference on Soil Mechanics and Foundation Engineering, Turkey, pp. 55–64 (1975)
6. Edil, T., Krizek, R., Zelasko, J.: Effect of grain characteristics on packing of sands. In: Proceedings of the Istanbul Conference on Soil Mechanics and Foundation Engineering, Istanbul, Turkey, pp. 46–54. Istanbul Technical University (1975)
7. Oda, M., Koishikawa, I., Higuchi, T.: Experimental study of anisotropic shear strength of sand by plane strain test. Soils Found. **18**(1), 25–38 (1978)
8. Sladen, J.A., D'Hollander, R.D., Krahn, J.: The liquefaction of sands, a collapse surface approach. Can. Geotech. J. **22**(4), 564–578 (1985)
9. Vepraskas, M.J., Cassel, D.K.: Sphericity and roundness of sand in coastal plain soils and relationships with soil physical properties. Soil Sci. Soc. Am. J. **51**(5), 1108 (1987)
10. Moroto, N., Ishii, T.: Shear strength of uni-sized gravels under triaxial compression. Soils Found. **30**(2), 23–32 (1990)
11. Sukumaran, B., Ashmawy, A.K.: Quantitative characterisation of the geometry of discret particles. Géotechnique **51**(7), 619–627 (2001)
12. Sukumaran, B., Ashmawy, A.K.: Influence of inherent particle characteristics on hopper flowrate. Powder Technol. **138**(1), 46–50 (2003)
13. Cubrinovski, M., Ishihara, K.: Maximum and minimum void ratio characteristics of sands. Soils Found. **42**(6), 65–78 (2002)
14. Yasin, S.J.M., Safiullah, A.M.M.: Effect of particle characteristics on the strength and volume change behavior of sand. J. Civil Eng. **31**(2), 127–148 (2003)
15. Santamarina, J.C., Cho, G.C.: Soil behaviour: the role of particle shape. In: Advances in Geotechnical Engineering: The Skempton Conference, London, pp. 604–617 (2004)
16. Cerato, A., Lutenegger, A.: Specimen size and scale effects of direct shear box tests of sands. Geotech. Test. J. **29**(6), 1–10 (2006)
17. Cho, G.-C., Dodds, J., Santamarina, J.C.: Particle shape effects on packing density, stiffness, and strength: natural and crushed sands. J. Geotech. Geoenviron. Eng. **132**(5), 591–602 (2006)
18. Guo, P., Su, X.: Shear strength, interparticle locking, and dilatancy of granular materials. Can. Geotech. J. **44**(5), 579–591 (2007)
19. Masad, E., Al-Rousan, T., Button, J., Little, D., Tutumluer, E.: Test methods for characterizing aggregate shape texture, and angularity. In: National Cooperative Highway Research Program Report 555. Transportation Research Board, Washington, DC (2007)
20. Rousé, P.C., Fannin, R.J., Shuttle, D.A.: Influence of roundness on the void ratio and strength of uniform sand. Géotechnique **58**(3), 227–231 (2008)
21. Bareither, C.A., Edil, T.B., Benson, C.H., Mickelson, D.M.: Geological and physical factors affecting the friction angle of compacted sands. J. Geotech. Geoenviron. Eng. **134**(10), 1476–1489 (2008)
22. Cavarretta, I., O'Sullivan, C., Coop, M.: The influence of particle characteristics on the behaviour of coarse grained soils. Géotechnique **60**(6), 413–423 (2010)
23. Shin, H., Santamarina, J.C.: Role of particle angularity on the mechanical behavior of granular mixtures. J. Geotech. Geoenviron. Eng. **139**(2), 353–355 (2013)
24. Zheng, J., Hryciw, R.D.: Index void ratios of sands from their intrinsic properties. J. Geotech. Geoenviron. Eng. 06016019. doi:10.1061/(ASCE)GT11.1943-5606.0001575 (2016)
25. Cundall, P.A.: A computer model for simulating progressive large scale movements in blocky rock systems. In: Proceedings of Proceedings of the Symposium of the International Society of Rock Mechanics. International Society for Rock Mechanics (ISRM) vol. 1, paper no. II-8, pp. 129–136 (1976)
26. Lin, X., Ng, T.T.: A three-dimensional discrete element model using arrays of ellipsoids. Géotechnique **47**(2), 319–329 (1997)
27. Mustoe, G.G.W., Miyata, M.: Material flow analyses of noncircular-shaped granular media using discrete element methods. J. Eng. Mech. **127**(10), 1017–1026 (2001)
28. Ouadfel, H., Rothenburg, L.: 'Stress-force-fabric' relationship for assemblies of ellipsoids. Mech. Mater. **33**(4), 201–221 (2001)
29. Ng, T.-T.: Particle shape effect on macro- and micro-behaviors of monodisperse ellipsoids. Int. J. Numer. Anal. Meth. Geomech. **33**(4), 511–527 (2009)
30. Fu, P., Dafalias, Y.F.: Fabric evolution within shear bands of granular materials and its relation to critical state theory. Int. J. Numer. Anal. Meth. Geomech. **35**(18), 1918–1948 (2010)
31. Pournin, L., Weber, M., Tsukahara, M., Ferrez, J.A., Ramaioli, M., Liebling, T.M.: Three-dimensional distinct element simulation of spherocylinder crystallization. Granular Matter **7**(2–3), 119–126 (2005)
32. Azéma, E., Radjaï, F., Peyroux, R., Saussine, G.: Force transmission in a packing of pentagonal particles. Phys. Rev. E **76**(1), 011301 (2007). doi:10.1103/PhysRevE.76.011301
33. Azéma, E., Radjaï, F.: Stress–strain behavior and geometrical properties of packings of elongated particles. Phys. Rev. E **81**(5), 051304 (2010). doi:10.1103/PhysRevE.81.051304
34. Azéma, E., Radjai, F., Saussine, G.: Quasistatic rheology, force transmission and fabric properties of a packing of irregular polyhedral particles. Mech. Mater. **41**(6), 729–741 (2009)
35. Galindo-Torres, S.A., Pedroso, D.M.: Molecular dynamics simulations of complex-shaped particles using Voronoi-based spheropolyhedra. Phys. Rev. E **81**(6), 061303 (2010). doi:10.1103/PhysRevE.81.061303
36. Mollon, G., Zhao, J.: 3D generation of realistic granular samples based on random fields theory and Fourier shape descriptors. Comput. Methods Appl. Mech. Eng. **279**, 46–65 (2014)
37. Ferellec, J.-F., McDowell, G.R.: A method to model realistic particle shape and inertia in DEM. Granular Matter **12**(5), 459–467 (2010)
38. Langston, P., Ai, J., Yu, H.: Simple shear in 3D DEM polyhedral particles and in a simplified 2D continuum model. Granular Matter **2013**(15), 595–606 (2013)
39. Boton, M., Azéma, E., Estrada, N., Radjaï, F., Lizcano, A.: Quasistatic rheology and microstructural description of sheared granular materials composed of platy particles. Phys. Rev. E **87**(3), 032206 (2013). doi:10.1103/PhysRevE.87.032206
40. Spellings, M., Marson, R.L., Anderson, J.A., Glotzer, S.C.: GPU accelerated Discrete Element Method (DEM) molecular dynamics

for conservative, faceted particle simulations. J. Comput. Phys. **334**, 460–467

41. Andrade, J.E., Lim, K.-W., Avila, C.F., Vlahinic, I.: Granular element method for computational particle mechanics. Comput. Methods Appl. Mech. Eng. **241–244**, 262–274 (2012)

42. Taghavi, R.: Automatic Clump Generation Based on Mid-Surface. In: Al, D.S.e. (ed.) Proceedings, 2nd International FLAC/DEM Symposium, Melbourne, pp. 791–797. Minneapolis: Itasca International Inc. (2011)

43. Zheng, J., Hryciw, R.D.: A corner preserving algorithm for realistic DEM soil particle generation. Granular Matter **18**(4), 1–18 (2016). doi:10.1007/s10035-016-0679-0

44. Wadell, H.: Volume, shape, and roundness of rock particles. J. Geol. **40**(5), 443–451 (1932)

45. Wadell, H.: Sphericity and roundness of rock particles. J. Geol. **41**(3), 310–331 (1933)

46. Wadell, H.: Volume, shape, and roundness of quartz particles. J. Geol. **43**(3), 250–280 (1935)

47. Barrett, P.J.: The shape of rock particles: a critical review. Sedimentology **27**(3), 291–303 (1980)

48. Tickell, F.G.: The Examination of Fragmental Rocks. Stanford University Press, Stanford, CA (1931)

49. Altuhafi, F., O'Sullivan, C., Cavarretta, I.: Analysis of an image based method to quantify the size and shape of sand particles. J. Geotech. Geoenviron. Eng. **139**(8), 1290–1307 (2013)

50. Krumbein, W.C., Sloss, L.L.: Stratigraphy and Sedimentation. W.H. Freeman and Company, San Francisco (1951)

51. Zheng, J., Hryciw, R.D.: Traditional soil particle sphericity, roundness and surface roughness by computational geometry. Géotechnique **65**(6), 494–506 (2015)

52. Zheng, J., Hryciw, R.D.: Roundness and sphericity of soil particles in assemblies by computational geometry. J. Comput. Civ. Eng. (2016). doi:10.1061/(ASCE)CP.1943-5487.0000578

53. Zheng, J., Hryciw, R.D.: Index void ratios of sands from their intrinsic properties. J. Geotech. Geoenviron. Eng. (2016). doi:10.1061/(ASCE)GT.1943-5606.0001575

54. Krumbein, W.C.: Measurement and geological significance of shape and roundness of sedimentary particles. J. Sediment. Petrol. **11**(2), 64–72 (1941)

55. Powers, M.C.: A new roundness scale for sedimentary particles. J. Sediment. Petrol. **23**(2), 117–119 (1953)

56. Hryciw, R.D., Zheng, J., Shetler, K.: Particle roundness and sphericity from images of assemblies by chart estimates and computer methods. J. Geotech. Geoenviron. Eng. (2016). doi:10.1061/(ASCE)GT.1943-5606.0001485

57. Rao, C., Tutumluer, E., Stefanski, J.A.: Coarse aggregate shape and size properties using a new image analyzer. J. Test. Eval. **29**(5), 461–471 (2001)

58. Rao, C., Tutumluer, E.: Determination of volume of aggregates: new image-analysis approach. Trans. Res. Record J Transp. Res. Board **1721**, 73–80 (2000)

59. Pan, T., Tutumluer, E., Carpenter, S.H.: Effect of coarse aggregate morphology on permanent deformation behavior of hot mix asphalt. J. Trans. Eng. **132**(7), 580–589 (2006)

60. Tutumluer, E., Pan, T.: Aggregate morphology affecting strength and permanent deformation behavior of unbound aggregate materials. J. Mater. Civ. Eng. **20**(9), 617–627 (2008)

61. Al-Rousan, T., Masad, E., Tutumluer, E., Pan, T.: Evaluation of image analysis techniques for quantifying aggregate shape characteristics. Constr. Build. Mater. **21**(5), 978–990 (2007)

62. Mahmoud, E., Masad, E.: Experimental methods for the evaluation of aggregate resistance to polishing, abrasion, and breakage. J. Mater. Civ. Eng. **19**(11), 977–985 (2007)

63. Fletcher, T., Chandan, C., Masad, E., Sivakumar, K.: Aggregate imaging system for characterizing the shape of fine and coarse aggregates. Transp. Res. Record J Transp. Res. Board **1832**, 67–77 (2003)

64. Chandan, C., Sivakumar, K., Masad, E., Fletcher, T.: Application of imaging techniques to geometry analysis of aggregate particles. J. Comput. Civil Eng. **18**(1), 75–82 (2004)

65. Ohm, H.-S., Hryciw, R.D.: Translucent segregation table test for sand and gravel particle size distribution. Geotech. Test. J. **36**(4), 20120221 (2013)

66. Zheng, J., Hryciw, R.D., Ohm, H.S.: Three-dimensional translucent segregation table (3D-TST) test for soil particle size and shape distribution. In: International Symposium on Geomechanics from Micro to Macro, London, pp. 1037–1042. Taylor & Francis Group, Abingdon (2014)

67. Raschke, S.A., Hryciw, R.D.: Vision cone penetrometer for direct subsurface soil observation. J. Geotech. Geoenviron. Eng. **123**(11), 1074–1076 (1997)

68. Ghalib, A.M., Hryciw, R.D., Susila, E.: Soil stratigraphy delineation by VisCPT. In: Innovations and Applications in Geotechnical Site Characterization, Reston, VA, pp. 65–79. ASCE, New York (2000)

69. Hryciw, R.D., Ohm, H.S.: Soil migration and piping susceptibility by the VisCPT. In: Geo-Congress, San Diego, CA, pp. 192–195 (2013)

70. Zheng, J., Hryciw, R.D.: Optical flow analysis of internal erosion and soil piping in images captured by the VisCPT. In: Geo-Shanghai 2014, Shanghai, China, pp. 55–64. ASCE, New York (2014)

71. Ohm, H.-S., Hryciw, R.D.: Size distribution of coarse-grained soil by sedimaging. J. Geotech. Geoenviron. Eng. (2014). doi:10.1061/(ASCE)GT.1943-5606.0001075, 04013053

72. Rosin, P., Rammler, E.: The laws governing the fineness of powdered coal. J. Inst. Fuel **7**, 29–36 (1933)

73. Itasca Consulting Group. Particle Flow Code in Two Dimensions.: User's Manual, Version 5.0.: Minneapolis, MN (2015)

74. Plimpton, S.: Fast parallel algorithms for short-range molecular dynamics. J. Comput. Phys. **117**(1), 1–19 (1995)

75. Kloss, C., Goniva, C., Hager, A., Amberger, S., Pirker, S.: Models, algorithms and validation for opensource DEM and CFD-DEM. Prog. Comput. Fluid Dyn. Int. J. **12**(2/3), 140–152 (2012)

76. Lings, M.L., Dietz, M.S.: An improved direct shear apparatus for sand. Géotechnique **54**(4), 245–256 (2004)

77. Jewell, R.A.: Direct shear tests on sand. Géotechnique **39**(2), 309–322 (1989)

78. Kokusho, T., Hara, T., Hiraoka, R.: Undrained shear strength of granular soils with different particle gradations. J. Geotech. Geoenviron. Eng. **13**(6), 621–629 (2004)